Available online at www.sciencedirect.com
SCIENCE DIRECT
Journal of Photochemistry and Photobiology A: Chemistry 176 (2005) 3–14
Journal of Photochemistry and Photobiology A:Chemistry
www.elsevier.com/locate/jphotochem

Absorption cross-section of IO at 427.2 nm and 298 K

T.J. Dillon, M.E. Tucceri, D. Hölscher, J.N. Crowley *

Max Planck Institut für Chemie, Division of Atmospheric Chemistry, Postfach 3060, 55020 Mainz, Germany

Available online 26 October 2005

Abstract

The absorption cross-section of the IO radical was determined at a wavelength of 427.2 nm and at a resolution of ≈0.08 nm at room temperature (298 ± 2 K) using the technique of laser photolysis combined with transient absorption spectroscopy. Three previously untested chemical schemes were used to generate calibrated amounts of IO and two of these were used to derive a cross-section of $\sigma^{IO}_{427.2\,nm} = (3.55 \pm 0.35) \times 10^{-7}$ cm^2 molecule^{-1}. The value of σ_{max}, at the peak of the 4,0 band (located at ≈427.08 nm, wavelengths given in air) is ≈8% larger than at 427.2 nm. This result is compared with previous determinations and evaluations. As part of this study the branching ratio (at 298 K) of IO formation from the reactions of O(^{3}P) with CF_3I and CH_3I were measured as 0.90 ± 0.05 and 0.38 ± 0.05, respectively. Data on the formation and relaxation of vibrationally excited IO in the chemical systems used in this study were also obtained.

Keywords: Iodine oxide; Absorption spectrum; Cross-section; Atmospheric chemistry; Photochemistry

1. Introduction

Recent observations of the IO radical in the marine boundary [1–3] layer provide evidence for the important role of iodine chemistry in the atmosphere. The release by marine algae of organic and inorganic iodine compounds such as e.g. CH_3I, CH_2I_2 and I_2 is believed to be the major source of iodine into the troposphere [4,5]. Degradation of these species by photolysis [6,7], reaction with OH [8] or Cl atoms [9] results in the release of I atoms, which react almost exclusively with O_3 to form the IO radical (R1). The IO radical is removed by photolysis (R2) and by reaction with itself (R3), HO_2 (R4), NO (R5) and NO_2 (R6).

$$I + O_3 \rightarrow IO + O_2 \quad (R1)$$

$$IO + h\nu \rightarrow I + O \quad (R2)$$

$$IO + IO \rightarrow \text{Products} \quad (R3)$$

$$IO + HO_2 \rightarrow HOI + O_2 \quad (R4)$$

$$IO + NO \rightarrow I + NO_2 \quad (R5)$$

$$IO + NO_2 + M \rightarrow IONO_2 + M \quad (R6)$$

Reactions (R2) and (R5) do not lead to net ozone loss, as O atoms formed directly in (R2), or indirectly via photolysis of NO_2 formed in (R5) react with O_2 to reform the O_3 lost in (R1). In contrast, the HOI product of (R4) is rapidly photolysed to form OH and I with a quantum yield of unity [10], which when combined with (R1) and (R4), represent a catalytic loss of O_3 [11]. Net, gas phase reaction schemes that destroy ozone can also be written for reaction (R3) (depending on the identity and photochemical fate of the products [12]), and (R6) (depending on the photochemistry of $IONO_2$). In addition, both HOI and $IONO_2$ are known to interact with sea salt to release photolabile, iodine containing, halogens [13,14].

The lifetime of IO with respect to photolysis (R2) and thus the partitioning of reactive iodine between IO and I depends on the absorption cross-sections in the visible part of its absorption spectrum, and on the quantum yield, which is close to unity [10,15].

The main features of the IO absorption spectrum are the strong vibrational bands of the $A^2\Pi \leftarrow X^2\Pi$ transition between about 400 and 470 nm, the first observation of which is attributed to Coleman et al. [16]. The vibrational bands show varying degrees of rotational structure, dependent on the predissociation lifetime of the upper state. The strongest features in the spectrum are the vibrational band head at ≈466 nm and further transitions within the same progression at (approximate wavelengths) 456 nm (1,0), 445 nm (2,0), 436 nm (3,0), 427 nm (4,0) and 421 nm (5,0). The 2,0 band displays substantial rotational

* Corresponding author. Tel.: +49 6131 305 436; fax: +49 6131 305 436.
E-mail address: crowley@mpch-mainz.mpg.de (J.N. Crowley).

1010-6030/$ – see front matter © 2005 Elsevier B.V. All rights reserved.
doi:10.1016/j.jphotochem.2005.09.025

structure [17] and has been used to detect IO by laser induced fluorescence [15,18] and cavity ringdown spectrocopy [19,20]. In contrast, the (4,0) band has no rotational structure. For this reason, and also because it is one of the strongest transitions at moderate resolution, the 4,0 band has been the most frequently employed for absorption spectroscopy. The presence of strong vibrational features in the IO spectrum has allowed measurements of IO in the atmosphere using the technique of differential absorption spectroscopy, which relies on accurate values of absorption cross-sections to convert measured column optical densities into concentrations. In addition, several laboratory studies of the important atmospheric reactions of IO (especially its self-reaction) have utilised absorption spectroscopic detection of IO, and have required absolute cross-sections to derive kinetic parameters.

Clearly, there is an urgent need for accurate cross-sections of the IO radical in order to assess its role in the chemistry of the marine boundary layer. However, as detailed below, there are significant discrepancies in the literature determinations of the cross-section of IO close to the maximum of the 4,0 band, commonly given as 427.2 nm. The cross-section at this wavelength has been used to place the relative spectrum of IO between ≈350 and 460 nm onto an absolute basis. It is unclear whether the causes of this poor agreement are spectroscopic in nature (e.g. resolution effects), or are related to uncertainties in the chemical schemes used to generate IO. The goal of the present study was to develop novel, quantifiable generation schemes for IO in order to extend the database on this important photochemical parameter.

2. Experimental

Several features of the experimental set-up were described in a previous publication [10,21]. In brief, the central component of the experimental set-up (Fig. 1) was a ≈130 cm long Pyrex tube (i.d. = 4 cm) which served as reaction vessel. Quartz end-windows were used to transmit light from the xenon lamp and the lasers. A small flow of gas purged the insides of these windows to prevent built up of solid deposits (often encountered in photochemical studies involving iodine oxides) which otherwise caused slight drifts in the transmitted light intensity. The lasers were coupled into the reaction cell via dielectric mirrors which were transmissive at the analysis light wavelengths (see caption to Fig. 1 for details). The analysis light was provided by a 75 W, high pressure xenon lamp, which was collimated, and apertured down to ≈5 mm before being directed (counter propagating to the lasers) on the main axis through the cell. The transmitted light was focussed onto the entrance slit of a 50 cm monochromator equipped with a 1200 lines/mm grating and a photomultiplier tube. This set-up was used for the detection of transient absorption signals at discrete, selected wavelengths. In these experiments it was important that the monochromator could accurately and reproducibly scan to the required wavelength. The calibration of the monochromator was therefore regularly checked by using the nearest line of a low pressure Hg Penray-lamp at 435.8 nm. Use of a relatively highly dispersive grating resulted in a wavelength reproducibility and accuracy

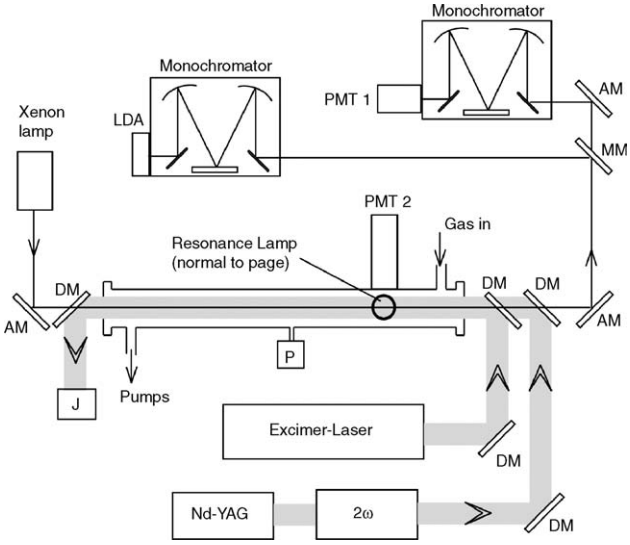

Fig. 1. Schematic diagram of the experimental set-up. AM, aluminium mirror; DM, dielectric mirror (coated for 193, 248, or 351/355 nm); MM moveable mirror; PMT1, 250–600 nm photomultiplier; PMT2, Vac-UV photomultiplier; LDA, linear diode array; J, joulemeter; P, pressure gauge.

of ≈0.05 nm. The effective resolution of the monochromator was determined by measuring the shape and half width of the 435.8 nm line from a low pressure mercury lamp at various entrance and exit slit widths.

After transmitting the cell, the analysis light could also be directed to a 25 cm monochromator, equipped with a 600 lines/mm grating and a linear diode array detector. In this configuration, the concentrations of stable species flowing through the cell (e.g. I_2) could be monitored over a wavelength range of ≈160 nm.

Pulsed photolysis at 193, 248 or 351 nm was provided by an excimer laser (Lambda-Physik LPX/Novatube); 355 nm photolysis was provided by a frequency tripled Nd–YAG laser (Quantel-Brilliant B). Careful alignment along the central axis of the cell ensured that the volume swept out by the laser light completely encompassed that of the analysis light. Typical flow rates in the cell were 5–6 L (STP) min^{-1} so that the contents of the reaction vessel were replaced between laser pulses (typically at ≈1 Hz) during measurement of transient absorption along the cell length.

For the transient absorption experiments, the PMT signal was amplified and transferred via a low-pass filter (≈0.1 MHz) to a digital oscilloscope for averaging, before transfer to a PC for storage and analysis. Typically, 128, 256 or 512 profiles were averaged to improve the signal-to-noise ratio.

A limited set of experiments were carried out to examine the role of vibrational excitation of IO using laser induced fluorescence. These experiments were carried out in a set-up that has been used previously for OH kinetic measurements [22] and recently adapted to detect IO [23]. Briefly, vibrationally relaxed IO($v = 0$) was detected by exciting the ($2 \leftarrow 0$) transition at ≈445.0 nm and IO($v = 1$) was detected by exciting the ($2 \leftarrow 1$) transition at 458.8 nm. These wavelengths were provided by a Nd–YAG pumped dye laser operating with coumarin 47 dye. Fluorescence from IO was detected by a photomultiplier

screened with a 490 cut-off filter. The reader is referred to Dillon et al. [23] for more details of this set-up.

2.1. Materials

Ozone was prepared in situ by passing a flow of pure O_2 over a low pressure "pen-ray" mercury lamp. A flow of I_2 was generated by passing N_2 through a U-tube containing I_2 at ambient temperature. CF_3I was added directly via a flow controller. The stated purities of the chemicals used were: I_2 (99.8%, Aldrich), CF_3I (99%, Aldrich), CH_3I (99.5%, Aldrich), CH_2I_2 (99%, Aldrich), He (99.996%, Messer), N_2 and O_2 (99.996%, Messer), NO_2 (99.5%, Aldrich). The I_2 was re-distilled prior to use, CF_3I was passed though a cold trap to remove any I_2, NO_2 was purified by degassing at 195 K to remove N_2, O_2 and NO.

2.2. Generation of IO

A number of IO generation schemes were employed in our studies of the absorption cross-section of IO, all of which used the reaction of $O(^3P)$ with either I_2 or CF_3I:

$$O(^3P) + I_2 \rightarrow IO + I \quad \text{(R7)}$$

$$O(^3P) + CF_3I \rightarrow IO + CF_3 \quad \text{(R8a)}$$

$$\rightarrow \text{Other products} \quad \text{(R8b)}$$

Reaction (R7) has a large rate coefficient [24] of 1.2×10^{-10} cm^3 molecule^{-1} s^{-1} and only one reaction channel, so that the amount of IO formed can be equated to that of $O(^3P)$ lost. For (R8) the rate coefficient at room temperature is 4.3×10^{-12} cm^3 molecule^{-1} s^{-1} [25,26] and a number of reaction channels exist [26]. The yield of IO per $O(^3P)$ reacted therefore depends on the branching ratio, k_{8a}/k_8, which was also checked as part of this study. The amount of $O(^3P)$ generated per laser pulse was measured in back-to-back experiments in which, under otherwise unchanged conditions of laser power and optical path, I_2 or CF_3I were replaced by O_2, and the yield of O_3 (R9) measured.

$$O(^3P) + O_2 + M \rightarrow O_3 + M \quad \text{(R9)}$$

The amount of O_3 formed was calculated from the measurement of optical density using a cross-section at 254 nm of 1.16×10^{-17} cm^2 molecule^{-1} [27].

The $O(^3P)$ atoms were generated either by the photolysis of O_2 (193 nm) or NO_2 (351 or 355 nm):

$$O_2 + h\nu(193\,\text{nm}) \rightarrow 2\,O(^3P) \quad \text{(R10)}$$

$$NO_2 + h\nu(351/355\,\text{nm}) \rightarrow O(^3P) + NO \quad \text{(R11)}$$

In addition, some experiments were carried out in which the photolysis of O_3 at 248 nm was used as $O(^3P)$ source as described in (R12) and (R13).

$$O_3 + 248\,\text{nm} \rightarrow O_2 + O(^1D) \quad \text{(R12)}$$

$$O(^1D) + N_2 \rightarrow O(^3P) + N_2 \quad \text{(R13)}$$

These experiments were designed primarily to investigate the shape of the 4,0 band of IO and the effect of spectral resolution, and not to derive absolute cross-sections. They were characterised by a very high chemical stability, which was achieved by generating O_3 in a constant flow of O_2 over a low pressure mercury "pen-ray" lamp.

Note that we did not use the 193 nm photolysis of N_2O in the presence of CF_3I or I_2 to generate IO, as this scheme has been widely used before (see Section 4).

3. Results

3.1. Shape of the 4,0 band and the effect of resolution

As mentioned above, most determinations of the IO cross-section have been made in the 4,0 band. Harwood et al. [28] measured the shape of this band at high resolution using a tunable diode laser, and found it to possess no rotational structure. The same authors found the maximum of the asymmetric band to be located at 427.2 nm, the quoted wavelength of their diode-laser, measured in vacuo. As our experiments were conducted using an air filled monochromator at atmospheric pressure, we expect a shift of −0.12 nm in the position of the maximum [29]. As the 4,0 band is asymmetric, the effect of resolution on the measured value of the cross-section will depend on the central wavelength. We, therefore, examined the shape and position of this band by stepping our monochromator in ≈30 discrete steps between 425 and 434 nm, with measurements of IO decay traces at each wavelength. For these experiments, the monochromator was set at a resolution of 0.1 nm. The IO generation scheme used was the photolysis of $\approx 10^{13}$ molecules cm^{-3} of O_3 at 248 nm in the presence of $\approx 5 \times 10^{14}$ molecules cm^{-3} I_2 at a total pressure of 60 Torr air or N_2 (R12), (R13), (R7).

IO profiles thus obtained at each wavelength were then analysed by least-squares fitting to the one obtained at 427.2 nm to extract the relative absorbance, which is directly proportional to the relative cross-section. Experiments at 427.2 nm were repeated intermittently in order to obtain a measure of the chemical stability of the IO generation scheme, which was better than 5% and showed no systematic drift with time. The results of these experiments are summarised in Fig. 2, which plots the relative absorbance at each wavelength. Once the data of Harwood et al. [28] has been shifted by the theoretical value of −0.12 nm, and a suitable *y*-scaling factor applied, the two datasets show reasonable agreement. Improved agreement could be obtained either by shifting our dataset by +0.04 nm or the Harwood et al. dataset by a further −0.04 nm. As the wavelength accuracy of the diode laser used by Harwood et al. [28] should be considerably better than that of our monochromator system, we choose to apply the +0.04 nm correction to our data, which is within the expected wavelength accuracy of our monochromator. From this dataset (Fig. 2), we see that the cross-sections at the minima between the 5,0 and 4,0 band (at ≈425 nm) and between the 3,0 and 4,0 band (at ≈433 nm) are very close to zero, with values of <4% that obtained at the 4,0 band maximum. This is consistent with the spectra obtained by Bloss et al. [12] and Laszlo et al. [30], which have relative cross-sections of $\sigma_{433\,\text{nm}}/\sigma_{427\,\text{nm}}$ of

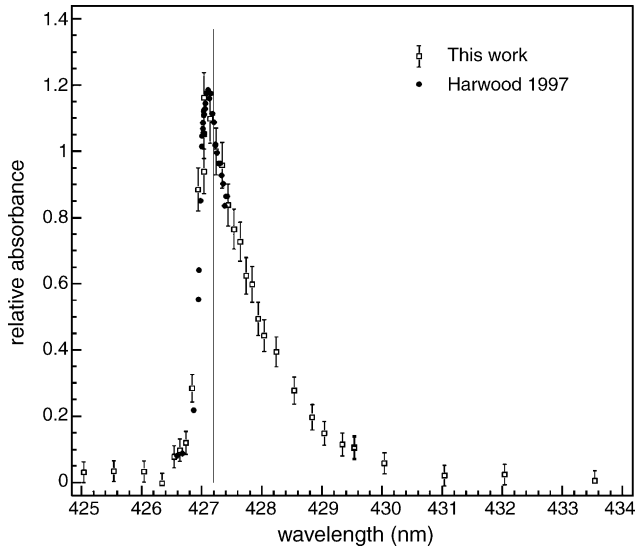

Fig. 2. The 4,0 band measured by Harwood et al. [28] and in this work. The Harwood et al. data, initially presented as in vacuo wavelengths have been shifted by −0.12 nm to enable comparison to the present dataset (see text for details).

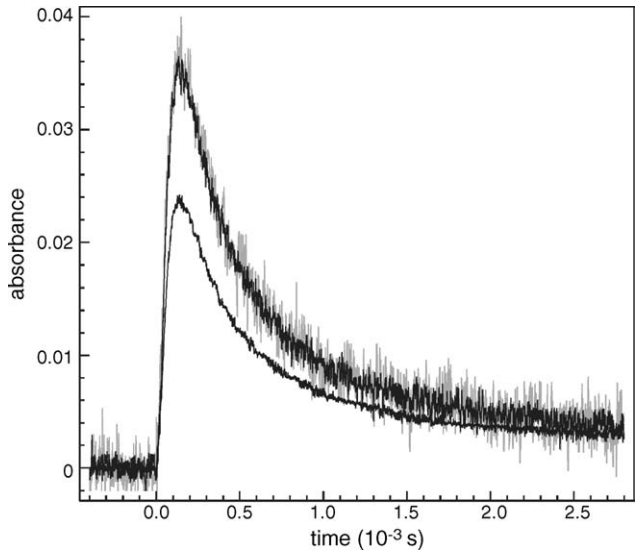

Fig. 3. Dependence of raw IO signal (absorbance) on spectral resolution at 427.2 nm. Raw data obtained at resolutions of 0.11 nm (noisy, grey trace), 0.19 nm (upper black trace) and 1.1 nm (lower trace).

≈0.03, but is smaller than that of Harwood et al. [28] who report $\sigma_{433\,nm}/\sigma_{427\,nm} = 0.1$ using a diode array spectrometer. Similar observations may be made for the cross-sections in the short wavelength minimum of the 4,0 band. As the diode array spectrum of Harwood et al. [28] was obtained at a higher spectral resolution than that of Bloss et al. [12] (0.44 nm versus 1.9 nm), the larger cross-sections in the band minima cannot be a result of poor resolution, but imply that the IO spectrum of Harwood et al. was contaminated with a broad, underlying absorber.

Having established the band shape, we went on to investigate the effect of resolution on the cross-section. Using a similar scheme to generate IO as described above, IO traces were obtained at different resolution, but fixed central wavelength of 427.2 nm. At this point it is useful to note that, for the asymmetric band, the position of the λ_{max} will shift to longer wavelengths as the resolution is decreased.

Raw data from a set of experiments are displayed in Fig. 3. As can be seen, the only change in the signals when varying the resolution from 0.11 to ≈0.19 nm is an increase in the signal-to-noise ratio owing to the increase in the light throughput. Within the scatter, which is determined by the chemical stability of the system, there is no reduction in the height of the initial optical density, nor the time dependence of the decay trace. In contrast, the IO trace obtained at a resolution of 1.1 nm has a significantly lower absorbance, indicating a change in the effective cross-section, which is accompanied by further improvement in the signal-to-noise ratio. Results obtained at a number of different resolutions are plotted in Fig. 4 in which the relative optical density (obtained by least squares fitting of data sets to each other) is plotted versus resolution. Only when the resolution is degraded to worse than 0.2 nm do we see a measurable decrease in optical density. The observation that the effect of resolution is rather weak supports the fact that the central wavelength of 427.2 nm is not at the maximum of the 4,0 band, but rather on a monotonically declining wing on the long wavelength side of the maximum. Measurements closer to λ_{max} would sample the rapidly decreasing cross-section on the short wavelength side of the maximum to reveal a stronger dependence on resolution. Conversely, measurements on the long wavelength side of the maximum will display a weaker dependence. This could be confirmed by showing that at 427.3 nm, the same absorbance trace (within experimental scatter) was recorded for resolutions of 0.1 and 0.4 nm.

This result, and the fact that many previous investigations of the cross-section quoted measurement wavelengths of 427.2 nm, guided our decision to make all subsequent cross-section measurements at 427.2 nm and at a resolution of ≈0.08 nm in the weakly resolution dependent plateau as shown in Fig. 4.

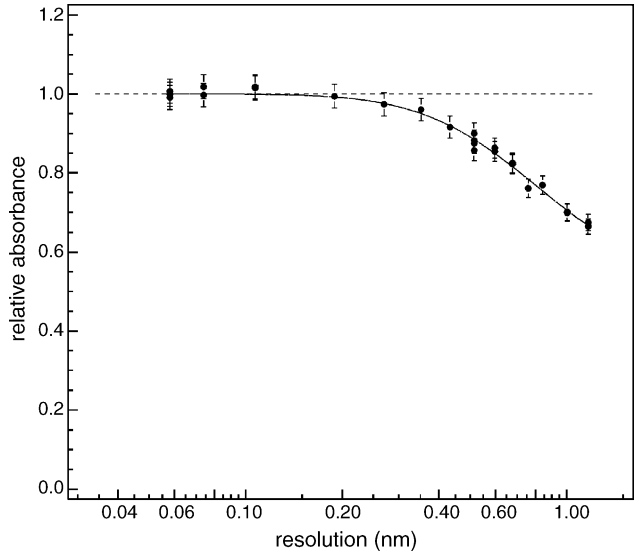

Fig. 4. Dependence of the absorbance of a constant amount of IO on variation in the spectrometer resolution at a central wavelength of 427.2 nm. The error bars represent an estimate (≈3%) of the chemical stability of the system (i.e. the reproducibility of the IO concentration).

3.2. Branching ratio for $O + CF_3I$

Use of reaction (R8) to generate known amounts of IO requires knowledge of the branching ratio k_{8a}/k_8. Gilles et al. [26], using LIF detection of IO, compared its formation in (R7) (yield of IO is assumed to be unity) with its formation in (R8) to derive $k_{8a}/k_8 = 0.83 \pm 0.09$ at 298 K and 100 Torr N_2 bath gas. No variation in branching ratio was found between 250 and 370 K at this pressure, and a temperature independent value of $k_{8a}/k_8 = 0.87$ may be obtained from a weighted average of the data presented in their Table 6.

Bloss et al.[12] examined the yield of IO from (R8), and found it to be independent of pressure between 50 and 760 Torr at 295 K. They did not carry out control experiments with reaction (R7) as external standard, thus the yields are presented relative to the yield at 100 Torr. In those experiments, a decrease in yield of ≈20% was observed as the pressure was increased from 100 to 760 Torr at 220 K, leading to speculation that a stabilised adduct, CF_3IO, could be formed.

In order to strengthen the database on this branching ratio, we have conducted back-to-back experiments in which the yield of IO from (R8) was compared to that from (R7). This is essentially the same procedure as employed by Gilles et al. [26], but is complementary in the sense that UV absorption spectroscopy rather than LIF was used to detect IO. For these experiments the photolysis of NO_2 at 351 nm was used as $O(^3P)$ source (R11), and back-to back experiments were carried out to determined the IO yield in (R8) relative to (R7) as a function of bath gas pressure. We also conducted some experiments on the formation of IO via reaction with CH_3I (R14).

$$O(^3P) + CH_3I \rightarrow IO + CH_3 \quad \text{(R14a)}$$

$$\rightarrow \text{Other products} \quad \text{(R14b)}$$

The experiments were carried out with adjustment of the relative concentrations of I_2 and RI such that the rates of reaction of $O(^3P)$ with RI (i.e. either CF_3I or CH_3I) and I_2 were roughly equal. This ensured similar production rates of IO, and, importantly, the same fractional loss of $O(^3P)$ due to reaction with NO_2, which was (10 ± 3)%. Under these conditions, the relative IO signals obtained using either I_2 or RI are directly proportional to the relative yields of IO from these reactions. Although CH_3I was not employed as an IO source in the cross-section determinations, owing to its low yield, the study of this reaction allowed us to test our methodology by providing the possibility for further comparison with the data of Gilles et al. [26], who also measured this parameter.

The raw data obtained for both CF_3I and CH_3I are qualitatively similar to that shown in Fig. 3, and as expected revealed smaller IO signals when $O(^3P) + CF_3I$ or $O(^3P) + CH_3I$ were used to generate IO compared to $O(^3P) + I_2$. The branching ratios at different pressures are listed in Table 1. No significant dependence on pressure was observed, and a weighted average of the data results in branching ratios (and associated statistical errors) of k_{8a}/k_8 and k_{14a}/k_{14} of 0.90 ± 0.05 and 0.38 ± 0.05, respectively. Given the different modes of $O(^3P)$ generation and IO detection employed, these results are in satisfactory agreement with those of Gilles et al. [26], who obtained $k_{8a}/k_8 = 0.87$ for CF_3I (see above) and 0.44 ± 0.04 for k_{14a}/k_{14} for CH_3I.

Table 1
Yields of IO in reactions of $O(^3P) + CF_3I$ and $O(^3P) + CH_3I$ at 298 K

$O(^3P) + CF_3I$ (R8)		$O(^3P) + CH_3I$ (R14)	
Pressure (Torr N_2)	IO yield[a]	Pressure (Torr N_2)	IO yield
31.2	0.82 ± 0.05	40	0.39 ± 0.04
58	0.90 ± 0.05	57	0.39 ± 0.03
97	0.90 ± 0.06	97	0.38 ± 0.03
147	0.93 ± 0.07		

[a] Average of up to three determinations at each pressure. The uncertainties are 2σ statistical errors.

3.3. IO cross-section at 427.2 nm

Altogether three chemical systems were used to generate IO and determine its cross-section at 427.2 nm. In each case, concentrations of reactants in the cell were determined by in situ optical absorption. NO_2 was monitored at 400 nm, ($\sigma^{NO_2}_{400\,nm} = 6.7 \times 10^{-19}$ cm^2 molecule^{-1}) [31], I_2 was monitored at 500 nm ($\sigma^{I_2}_{500\,nm} = 2.19 \times 10^{-18}$ cm^2 molecule^{-1}) [32] and CF_3I was monitored at 260 nm ($\sigma^{CF_3I}_{260\,nm} = 6.31 \times 10^{-19}$ cm^2 molecule^{-1}) [33]. The concentration of O_2 was calculated from its flow and the total flow and pressure in the reactor.

3.4. Scheme 1: (R11) + (R7)

A set of four experiments was conducted using photolysis of NO_2 (R11) as $O(^3P)$ source and reaction with I_2 (R7) to convert $O(^3P)$ rapidly to IO. Typical data from an experiment at 300 Torr total N_2 pressure and 298 K are displayed in Fig. 5. Initially an IO trace was obtained at 427.2 nm by photolysing ≈10^{14} molecules cm^{-3} of NO_2 in the presence of $(6–20) \times 10^{14}$ molecules cm^{-3} I_2. This results in rapid IO formation with conversion of $O(^3P)$ complete in <30 μs. IO then decays on a ms time scale largely due to its self-reaction, with a small contribution from reaction with NO_2. Note that the data collected within 50–60 μs after the laser pulse were influenced by scattered laser light, which prevented measurement of the rise part of the IO signal. In addition, a time independent, post-laser offset from loss of I_2 or NO_2 (OD ≈2×10^{-4}) could be observed by measuring the optical density change at 434 nm, an IO absorption minimum adjacent to the 4,0 band. For this reason, each measurement at 427.2 nm was accompanied by one at 434 nm, which was subtracted. Note that the cross-sections obtained are therefore differential cross-sections between the 4,0 band and its nearest, long wavelength minima, although we have shown (Fig. 2) that the absorption cross-section of IO at 434 nm is very close to zero.

In a back-to-back experiment, I_2 was then switched out of the reactor and the main flow of N_2 replaced with O_2. The experiment was repeated and the formation of O_3 from reaction (R9) was monitored at 254 nm (lower experimental trace in Fig. 5).

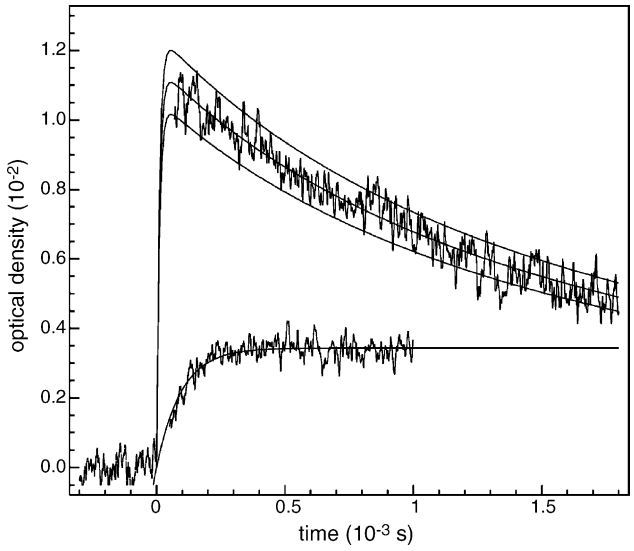

Fig. 5. Optical density changes due to the formation of O_3 (254 nm, lower experimental trace) and IO (427.2 nm, upper experimental trace) in the reactions of $O(^3P)$ with O_2 and I_2, respectively. The ozone trace was fit to a kinetic expression describing the pseudo-first order production (see text). The smooth lines on the IO trace are numerical simulations using IO cross-sections of 3.3×10^{-17} cm^2 molecule^{-1} (lower) 3.6×10^{-17} cm^2 molecule^{-1} (central) and 3.9×10^{-17} cm^2 molecule^{-1} (upper), respectively.

The O_3 trace was recorded at reduced resolution (0.4 nm) to improve signal-to-noise.

As found at 427.2 nm, correction had to be applied to remove the effects of laser stray light. This was carried out by measuring optical density changes at 254 nm in an experiment in which no O_2 was present, and no O_3 formation was possible. In both experiments the laser fluence (averaged over 100 laser shots) was monitored at the exit of the cell to confirm that no drift in intensity had occurred.

The amount of O_3 generated was obtained by fitting the corrected optical density trace at 254 nm to a first-order kinetic expression describing its formation:

$$[O_3]_t = [O_3]_{inf}(1 - \exp(-k_9[O_2]t) \quad \text{(i)}$$

where $[O_3]_t$ is the concentration of O_3 at time = t after the laser flash $[O_3]_{inf}$ is the O_3 concentration after the reaction has gone to completion and, in the absence of loss processes for $O(^3P)$ other than (R9), is equivalent to the initial $O(^3P)$ concentration. k_9 is the rate coefficient for reaction of $O(^3P)$ with O_2 at the pressure of the experiment (100, 150 or 300 Torr) and 298 K and $[O_2]$ is the oxygen concentration. The relationship between $[O_3]$ and the measured optical density changes at 254 nm is given by Beer's law:

$$OD_{254\,nm} = [O_3]l\,\sigma^{O_3}_{254\,nm} \quad \text{(ii)}$$

where $\sigma^{O_3}_{254\,nm}$ is the absorption cross-section of O_3 at 254 nm, and was taken to be 1.16×10^{-17} cm^2 molecule^{-1} [27]. The amount of O_3 formed cannot however be exactly equated to the initial amount of $O(^3P)$ as some will be lost in reaction with NO_2.

$$O(^3P) + NO_2 \rightarrow NO + O_2 \quad \text{(R15)}$$

The pseudo first-order loss rate coefficient for $O(^3P)$ due to reaction with NO_2 is given by $k_{15}[NO_2]$. Using $k_{15} = 1.0 \times 10^{-11}$ cm^3 molecule^{-1} s^{-1} at 298 K [34] and a typical NO_2 concentration of $(6–16) \times 10^{13}$ molecules cm^{-3}, this results in a loss rate coefficient of between 600 and 1600 s^{-1}. By comparison, the loss rate coefficient for reaction with O_2 was close to 13,000 s^{-1}, resulting in a maximum correction of $\approx(10 \pm 2)$%. The errors associated with this correction factor are based on uncertainty in the room temperature rate coefficients for (R15) and (R9), which are very well known, and the NO_2 and O_2 concentrations, which are known to better than 10%.

In conditions where $k_7[I_2] \gg k_{15}[NO_2]$, the initial concentration of $O(^3P)$ generated in the laser pulse can be equated to the initial concentration of IO and thus used to convert optical density measurements to a cross-section of IO at 427.2 nm. Typically, concentrations of $(4–12) \times 10^{14}$ molecules cm^{-3} of I_2 were used, resulting in $O(^3P)$ loss rates of $(5.7–16.5) \times 10^4$ s^{-1}. The loss rate of $O(^3P)$ with respect to reaction with NO_2 (present at between $(6–14) \times 10^{13}$ molecules cm^{-3}) was at most 1% of that due to (R7) and thus can be neglected. However, a combination of non-instantaneous IO formation with a rapid self reaction and the fact that data could not be obtained directly after the laser pulse makes extraction of the initial optical density due to IO rather uncertain. This is further compounded by increased uncertainty from extrapolation of second-order decay to $t = 0$, especially if the decay is mixed order due e.g. to reaction of IO with NO_2. For these reasons we have conducted numerical modelling of the reaction scheme to generate synthetic IO traces with which to compare our experimental data. The input parameters were the initial $O(^3P)$ concentration, the NO_2 and I_2 concentrations, and the set of reactions and rate coefficients listed in Table 2. Fig. 5 shows the result of three such simulations, in which the cross-section of IO is set to 3.3, 3.6 or 3.9×10^{-17} cm^2 molecule^{-1}. The simulation faithfully reproduces the initial height and time dependence of the IO radical trace when a cross-section of 3.6×10^{-17} cm^2 molecule^{-1} is used. Four experiments conducted at three different pressures (100–300 Torr) and using initial $O(^3P)$ and thus IO concentrations that varied by a factor of 2.6 gave similar results, which are listed in Table 3. The average value of the cross-section from experiments using this chemical system is thus $(3.6 \pm 0.3) \times 10^{-17}$ cm^2 molecule^{-1}.

Table 2
Reaction scheme used to simulate the experimental data

Reaction	Rate coefficient[a]	Reference
$O(^3P) + I_2 \rightarrow IO + I$	1.2×10^{-10}	[24]
$O(^3P) + CF_3I \rightarrow IO +$ products	$4.3 \times 10^{-12} \times 0.87$	[25,26]
$O(^3P) + NO_2 \rightarrow NO + O_2$	1.0×10^{-11}	[34]
$O(^3P) + IO \rightarrow I + O_2$	1.4×10^{-10}	[34]
$IO + IO \rightarrow$ products	9.9×10^{-11}	[34]
$IO + NO_2 + M \rightarrow IONO_2 + M$	$(1.5–2.4) \times 10^{-12}$[b]	[44]
$IO + NO \rightarrow I + NO_2$	1.95×10^{-11}	[34]
$O(^3P) + O_2 + M \rightarrow O_3 + M$	5.8×10^{-34} [M]	[34]

[a] Units of cm^3 molecule^{-1} s^{-1}.
[b] Depending on pressure.

Table 3
Summary of cross-sections derived in the present experiments

Scheme	Pressure (Torr)	$[O(^3P)]$[a]	$\sigma^{IO}_{427.2\,nm}$[b]
NO_2/I_2 (351 nm)	100	2.33	3.7 ± 0.3
	300	4.86	3.65 ± 0.25
	150	2.39	3.6 ± 0.4
	150	1.83	3.4 ± 0.25
NO_2/CF_3I (351 nm)	150	2.53	3.8 ± 0.55
	150	1.86	3.5 ± 0.5
	150	1.86	3.6 ± 0.55
NO_2/CF_3I (355 nm)	150	1.16	3.8 ± 0.6
	150	1.38	3.35 ± 0.45
	150	1.71	3.3 ± 0.5
O_2/CF_3I (193 nm)	105	4.85	3.3 ± 0.4
	90	4.43	4.0 ± 0.4
	100	6.22	3.2 ± 0.3

[a] Units of 10^{12} molecules cm^{-3}.
[b] Errors include estimated systematic uncertainty as discussed in the text.

3.5. Scheme 2: (R11) + (R8)

A further set of six experiments were conducted at 150 Torr and 298 K using the same scheme to generate $O(^3P)$, either using an excimer laser at 351 nm or a YAG laser at 355 nm to photolyse NO_2, but using reaction (R8) as the IO source. The extraction of the initial $O(^3P)$ concentration was identical to that described above, and the determination of the cross-section differed only in that the numerical simulation contained the 298 K rate coefficient and IO yield for reaction between $O(^3P)$ and CF_3I instead of $O(^3P)$ with I_2, and was initialised with the measured CF_3I concentration rather than that of I_2.

The concentrations of CF_3I and NO_2 were typically, $(5–10) \times 10^{16}$ molecules cm^{-3} and $(6–10) \times 10^{13}$ molecules cm^{-3}, respectively. Using the rate coefficients listed in Table 2, this implies that in all experiments >97% of the $O(^3P)$ would have reacted with CF_3I. The O_3 and IO traces measured in these experiments were qualitatively similar to those using $O(^3P) + I_2$ and are not shown. The values of $\sigma^{IO}_{427.2\,nm}$ derived are listed in Table 3 and seen to vary between 3.3 and 3.8×10^{-17} cm^2 $molecule^{-1}$, with an average value of 3.55×10^{-17} cm^2 $molecule^{-1}$. This result is in excellent agreement with that obtained using (R7) as IO source.

3.6. Scheme 3: (R10) + (R8)

Experiments were also carried out using the photolysis of O_2 at 193 nm as $O(^3P)$ source, as described above. In this case, only CF_3I was used to convert $O(^3P)$ to IO, as I_2 would be photolysed strongly at 193 nm. On paper, this is a rather chemically clean source of IO as no extra reactive species are involved, however, as in the experiments at 351 and 355 nm, a post laser pulse offset was observed in the absence of O_2 (i.e. in N_2 bath gas where no O_3 production is possible). This was especially large at 254 nm, the wavelength at which O_3 was monitored, where it amounted to up to 50% of the overall change in OD Some of this was most likely due to photolysis of air at 193 nm, which generates O_3 outside of the absorption vessel. The subsequent correction introduced significant error into the calculation of the initial $O(^3P)$ concentration, and therefore only a limited set of data were recorded using this technique. Once the $O(^3P)$ concentration had been established by photolysing O_2 at 193 nm, CF_3I was added and the monitoring wavelength shifted to 427.2 nm. With unchanged laser energy, an IO profile was then obtained.

The data were then simulated using the reaction scheme listed in Table 2, which takes into account the partitioning of $O(^3P)$ between reaction with CF_3I and O_2, and also the branching ratio of IO formation from reaction (R8). High concentrations of CF_3I were used to scavenge most of the $O(^3P)$. Typical initial concentrations of CF_3I of $(1.2–1.8) \times 10^{16}$ molecules cm^{-3} and O_2 pressures of close to 100 Torr, resulted in ≈90% of the $O(^3P)$ reacting with CF_3I. The results of these experiments are also summarised in Table 3. The limited data set shows more experiment-to-experiment scatter that those obtained using NO_2 photolysis, but returns an average value of 3.5×10^{-17} cm^2 $molecule^{-1}$, in good agreement with the other determinations of the cross-section.

The errors quoted in Table 3 include the upper and lower bounds of the numerical simulations, as shown in Fig. 5, and also include an estimate of systematic error, which differs from one type of experiment to the next. In all experiments, uncertainty in the IO cross-section determination arises from the error associated with the $O(^3P)$ measurement, which is mainly related to uncertainty in the O_3 cross-section at 254 nm (<5%) and the statistical error on measuring the optical density change at 254 nm, including post laser pulse stray light correction (4%). Errors that are related to the use of a numerical simulation to extract the cross-section of IO are largely determined by the branching ratio k_{8a}/k_8 in those experiments where CF_3I was used. Given the good agreement with the present study ($k_{8a}/k_8 = 0.9 \pm 0.05$), and with that of Gilles et al, ($k_{8a}/k_8 = 0.87 \pm 0.06$) which were conducted using completely different IO formation and detection schemes, we estimate the overall uncertainty of k_{8a}/k_8 to be about 10%. Uncertainties at the 20–30% level associated with the rate coefficients listed in Table 2 are insignificant for the NO_2 photolysis experiments as the partitioning of $O(^3P)$ between the reactant I_2 or CF_3I and the NO_2 is very strongly in favour of IO formation (see above) and changes of even a factor of two in e.g. the rate constant for reaction of $O(^3P)$ with I_2 or NO_2 would not be significant. This is slightly more critical for the 193 nm experiments, as only 90% of the $O(^3P)$ reacts to form IO. However, as discussed above, the rate coefficients for $O(^3P)$ with CF_3I and $O(^3P) + O_2$ are well known as are the reactor concentrations of CF_3I and O_2. Having established the obvious sources of uncertainty, we present an average value of $\sigma^{IO}_{427.2} = (3.55 \pm 0.35) \times 10^{-17}$ cm^2 $molecule^{-1}$ obtained in the experiments using NO_2 photolysis as $O(^3P)$ source. The data obtained from the 193 nm photolysis of O_2 are considered less reliable, and show more scatter, but are consistent with this result.

4. Discussion

4.1. Role of vibrational excitation of IO

Readily identified potential sources of systematic error such as e.g. uncertainty in the O_3 cross-sections or the branching ratio for IO formation in reaction (R8) (which both propagate directly through to the IO cross-section) have been discussed above. We now also consider the potential role of formation of vibrationally excited IO in the reactions used to generate it, i.e. (R7) and (R8). This would pose a problem if a significant fraction of IO is formed vibrationally excited, and if it were sufficiently long-lived to sequester IO on the time scale of our experiments. In this case, equating the initial O atom concentration to the initial IO concentration would lead to an underestimation of the true cross-section of IO($v = 0$). We first note that, according to the Boltzman expression, and using a IO vibrational frequency of $\approx$700 cm^{-1} [35], the equilibrium concentration of IO($v = 1$) at 298 K is expected to be of the order of 3% of IO($v = 0$). Using evaluated enthalpies of formation [34] we calculate the reaction enthalpies for (R7) and (R8a) as -88 and -10 kJ mol^{-1}, respectively. By comparison, the reaction of I atoms with O_3 is exothermic by 134 kJ mol^{-1}. For reaction (R8a), the excess energy available (10 kJ mol^{-1} $\approx$800 cm^{-1}) is barely greater that required to form IO($v = 1$), and it is unlikely that a significant fraction of the IO product is formed in a vibrationally excited state. However, as noted above, the yield of IO in (R8) (or k_{8a}/k_8) has been derived by comparison to the yield of IO in the reaction of O(^{3}P) with I_2, which may generate significant amounts of IO($v > 0$). If this were the case, then the branching ratio of k_{8a}/k_8 thus derived is too low.

In order to investigate this possibility we employed a separate experimental set-up to directly detect IO($v = 1$) by laser induced fluorescence (LIF) (see Section 2). IO($v = i$) was generated by the 351 nm photolysis of NO_2 in the presence of I_2 in He or N_2 bath gas and IO($v = 1$) was detected by exciting the ($2 \leftarrow 1$) transition. Typical reagent concentrations were: [NO_2] = (0.3–1.7) $\times$ 10^{14} molecule cm^{-3}, [I_2] = (0.8–4.7) $\times$ 10^{14} molecule cm^{-3} at pressures of 10–60 Torr.

The IO (2,1) excitation spectrum, which was measured as part of this work, is displayed in Fig. 6A and is in qualitative agreement with the spectrum presented by Turnipseed et al. [18] The relative shape of the spectrum showed no variation with time delay ($\approx$10–500 μs) after generation of O(^{3}P), and was thus rotationally thermalised.

A typical example of a time resolved IO($v = 1$) trace, obtained by excitation at the bandhead ($\approx$458.7 nm), is displayed in Fig. 6B. IO($v = 1$) is generated rapidly, at a rate which was consistent with its formation in the reaction of O(^{3}P) with I_2, and decays within $\approx$150 μs to a steady concentration, presumably determined by its equilibrium with vibrationally relaxed IO($v = 0$), which does not decay significantly on the time scale of these experiments. For comparison, a IO($v = 0$) profile, excited at $\approx$445.0 nm and measured back-to-back with IO($v = 1$) is also displayed. The poor signal-to-noise ratio for IO($v = 0$) is partially due to use of a laser dye that favoured excitation at 459 nm rather than 445 nm. From this dataset we can conclude that IO($v = 1$) is indeed formed in the reaction of O(^{3}P) with I_2 in the present chemical system and that its quenching lifetime is of the order of 100 μs. The lifetime of IO($v = 1$) was independent of using He or N_2 bath gas or the concentration of NO_2, suggesting that quenching by I_2 was dominant and implying a close to collisional quenching rate constant. Whatever the nature of the quenching process, this data clearly shows that in the experiments described above to measure the cross-sections of IO, which were conducted under similar conditions, only thermally equilibrated amounts of IO($v = 1$) were present. A close examination of the data in Fig. 6 shows that neither the IO($v = 0$) nor the IO($v = 1$) kinetics are well described by simple exponential expressions at short reaction times, suggesting that excitation of higher vibrational levels occurs, and that these are sequentially quenched (i.e. via $v = 2$, $v = 1$ etc.) to the groundstate.

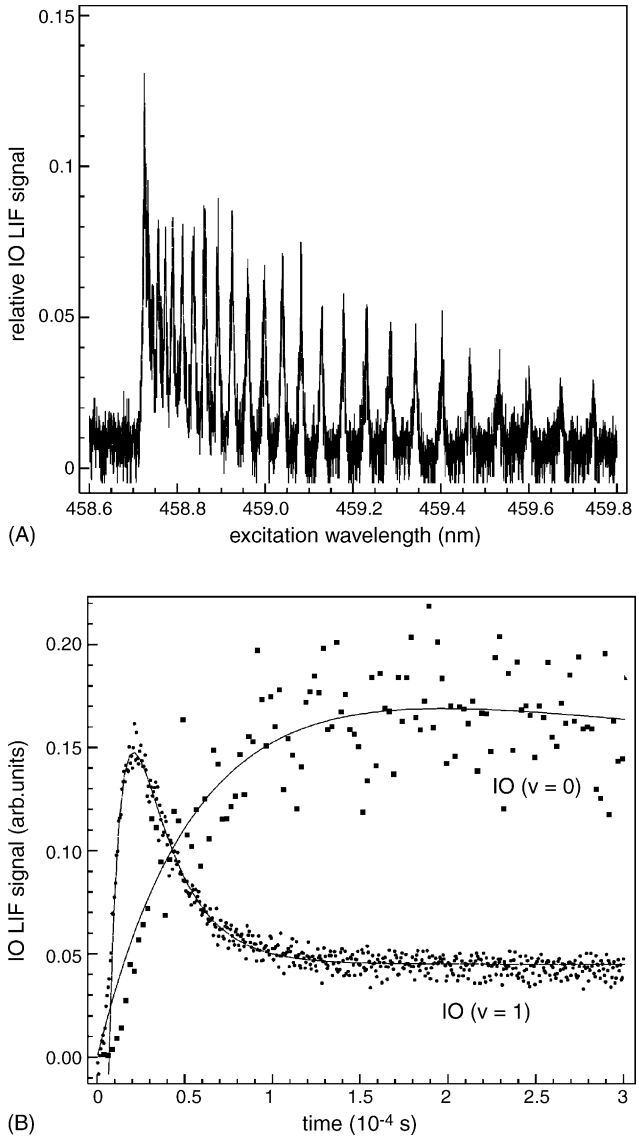

Fig. 6. (A) Fluorescence excitation spectrum of IO($v = 1$) with detection at $\lambda > \approx$490 nm. (B) Formation and decay of IO($v = 0$) and IO($v = 1$) using $\approx$445.0 and $\approx$458.7 nm as excitation wavelengths, respectively. The solid lines are fits to the data using a bi-exponential function ($v = 0$) and a multiple-exponential function ($v = 1$), respectively.

We also conducted similar experiments to search for formation of vibrationally excited IO in the reactions of $O(^3P)$ with CF_3I, CH_3I or CH_2I_2 and also in the reaction of I with O_3. In none of these experiments were we able to observed non-equilibrated amounts of vibrationally excited IO. This does not imply that it was not formed, but that that the quenching processes in each chemical system were significantly more rapid that the formation of IO.

In addition to the experiments on IO($v = 1$) described above, a number of further indirect observations confirm that perturbations due to IO($v > 0$) are unlikely to be significant. Using the reaction of $O(^3P)$ with I_2, we have recorded IO decay traces that closely obey second-order kinetics, at pressures between 20 and 600 Torr N_2. This would appear to preclude the presence of a significant amount of vibrationally hot IO which relaxes on the same time scale as the chemical lifetime of IO. We also note that experimental studies of the IO + NO reaction carried out in at low pressures of N_2 or using He bath gas have indeed reported unexpected behaviour, presumably due to slow vibrational relaxation of IO [36,37]. These same studies report that this problem is removed by using N_2 bath gas as pressures of >60 Torr.

4.2. Comparison with literature

In this section, we compare our absorption cross-section at 427.2 nm with other measurements that have been reported for the 4,0 band, and which span more than two decades of research. The literature values for IO cross-sections are listed in Table 4, which separates the measurements into those conducted at 427.2 nm, and those conducted at the peak of the 4,0 band. Early studies on IO were able to identify its absorption spectrum and assign transitions [38–40]. These were followed by the first quantitative determination of the absorption cross-section by Cox and Coker [41] in 1983, who used the 254 nm modulated photolysis of CH_3I in the presence of O_3 as source of IO ((R15) and then (R1)).

$$CH_3I + h\nu \rightarrow CH_3 + I \quad \text{(R15)}$$

Determination of the cross-section of $3.1^{+2.0}_{-1.5} \times 10^{-17}$ cm^2 molecule^{-1} was by kinetic analysis of the IO absorption trace at a quoted wavelength of 426.9 nm (resolution of 0.27 nm). These authors also scanned through the IO spectral features to find the maxima of the vibrational bands between 415–470 nm. They observed the maximum of the 4,0 band at the quoted wavelength of 426.9 nm, indicating a monochromator wavelength offset of about 0.2 nm. For this reason, we cite their result in Table 4 as having been taken at the maximum of the 4,0 band. This work was followed by similar experiments using a different photochemical source of IO, the photolysis of NO_2 at 350 ± 50 nm, with $O(^3P)$ scavenged efficiently by I_2 [42] i.e. reactions (R11) and (R7). A more straightforward determination of the rate of $O(^3P)$ production (and thus the rate of IO production) from NO_2 photolysis led the authors to prefer the cross-section thus obtained $(2.2 \pm 0.5) \times 10^{-17}$ cm^2 molecule^{-1} over the earlier work. It appears that in this study, the wavelength

Table 4
Previous determinations of IO cross-sections

Reference	σ(427.2) (10^{-17} cm^2)	σ(4,0)[a] (10^{-17} cm^2)	Resolution (nm) (fwhm)	IO source	Calibration
Cox and Coker [41]		$3.1^{+2.0}_{-1.5}$	0.27	$CH_3I + h\nu/O_3$	Kinetic analysis
Jenkin and Cox [42]		2.2 ± 0.5[b]	0.27	$NO_2 + h\nu/I_2$	ΔNO_2
Sander [43]	3.1 ± 0.3[c]	3.3 ± 0.3[d]	0.17	$O_2 + h\nu/I_2$	$O + O_2 \rightarrow O_3$
Stickel et al. [17]		3.1 ± 0.6[e]	0.01	$O_3 + h\nu/I_2$	Laser fluence
Laszlo et al. [30]	2.8 ± 0.5[f] 3.6 ± 0.6[g]	3.8 ± 0.7[d]	0.3	$N_2O + h\nu/I_2$	ΔI_2
Harwood et al. [28]		3.3 ± 0.7[h]	0.14	N_2O $h\nu/I_2$	ΔI_2
		3.6 ± 0.5[i]	0.14	$N_2O + h\nu/CF_3I$	$O + O_2 \rightarrow O_3$
		3.4 ± 0.4[j]	Diode laser	$O_3 + h\nu/I_2$	$HNO_3 + h\nu \rightarrow NO_2$
Bloss et al. [12]		1.9 ± 0.17[k]	1.13	$N_2O + h\nu/CF_3I$	$O + O_2 \rightarrow O_3$
This work	3.55 ± 0.35[c]	3.8 ± 0.4[d]	0.08	$NO_2 + h\nu/I_2$	$O + O_2 \rightarrow O_3$
				$NO_2 + h\nu/CF_3I$	$O + O_2 \rightarrow O_3$

[a] The maximum of the 4,0 band is at 427.2 nm in vacuo, or 427.08 nm in air. Note that at reduced resolution, the apparent position of λ_{max} will move to longer wavelength.
[b] Errors are 2σ (random).
[c] Errors are 2σ (random + systematic).
[d] Cross-section at 427.2 nm multipled by 1.08 to obtain cross-section at λ_{max}.
[e] Using a tunable dye laser.
[f] Errors are 2σ (random).
[g] Recalculated using the I_2 spectrum of Tellinghuisen [32] to calibrate the IO concentration and after correction for resolution effects.
[h] Errors are 1σ (random + 15% systematic).
[i] Errors are 1σ (random + 10% systematic).
[j] Errors are 1σ (random).
[k] Errors are 2σ (random + systematic error on yield of IO from $O(^3P) + CF_3I$).

quoted (426.9 nm), was taken from the previous investigation and potentially subject to an non-quantified drift in the wavelength offset (personal communication with Jenkin and Cox). This would help to explain the differences in cross-section reported in these two studies from the same laboratory.

Sander [43] determined IO cross-sections at 427.2 nm using the flash photolysis of O_2 to generate $O(^3P)$ (R10), which was then scavenged by I_2 to form IO (R7). Calibration of the initial $O(^3P)$ concentration was achieved by replacing I_2 with sufficient O_2 to stoichiometrically convert $O(^3P)$ to O_3 (R9). The cross-section obtained was $(3.1 \pm 0.3) \times 10^{-17}$ cm^2 molecule^{-1} at 298 K, and displayed a significant, negative dependence on temperature. A similar value for the cross-section was obtained by Stickel et al. [17], who employed the 248 nm laser photolysis of O_3 to form $O(^3P)$ and used I_2 to convert it to IO ((R12) followed by (R7)). Calibration of the initial $O(^3P)$ concentration was by measurement of laser fluence at 248 nm, and knowledge of the O_3 concentration. Laszlo et al. [30] also used the reaction of $O(^3P)$ with I_2 to generate IO, but employed a different source of $O(^3P)$, the 193 nm photolysis of N_2O in N_2 bath gas to generate $O(^3P)$.

$$N_2O + h\nu(193\,\text{nm}) + N_2 \rightarrow N_2 + O(^3P) \quad \text{(R16)}$$

Calibration of the initial IO concentration was obtained by equating its initial concentration to the loss of I_2 (R7) which was monitored simultaneously at 530 nm (using $\sigma(I_2) = 2.56 \times 10^{-18}$ cm^2 molecule^{-1}). These authors report a value of $(2.8 \pm 0.5) \times 10^{-17}$ cm^2 molecule^{-1} for the cross-section of IO at 427.2 nm at a resolution of 0.3 nm.

Harwood et al. [28] used three different chemical schemes to generate and calibrate IO and determine its cross-section in the 4,0 band. The experiments were carried out using either a monochromator operating at a spectral resolution of 0.14 nm, or using a diode laser with a 10^5 Hz bandwidth as light source and a photodiode as detector. Before discussing their data it is important to note that, when using a monochromator, and similar to the works of Cox and Coker [41] and Jenkin and Cox [42] these authors generally scanned around 427.2 nm to find the wavelength at which the absorption due to IO maximised, i.e. they always measured at the peak of the 4,0 band (personal communication with J. Burkholder). As we have seen above, in an air filled monochromator λ_{max} will be at 427.08 nm, and not at 427.2 nm. Thus, although these authors quote 427.2 nm as the measurement wavelength, it was most probably closer to 427.08 nm.

In essentially identical experiments to Laszlo et al. [30], using N_2O photolysis at 193 nm in the presence of I_2, Harwood et al. [28] obtained a cross-section of $(3.3 \pm 0.4) \times 10^{-17}$ cm^2 molecule^{-1} at 0.14 nm resolution. These experiments required substantial correction to the change in I_2 following the laser pulse, which was due not only to the reaction of $O(^3P)$ with I_2, but, in some experiments, predominantly due to direct photolysis at 193 nm.

The photolysis of N_2O in the presence of CF_3I was also used by Harwood et al. [28] to generate IO ((R16) followed by (R8)), but with its concentration defined by the initial $O(^3P)$ concentration (determined by monitoring O_3 formation when CF_3I was replaced by O_2) and knowledge of the branching ratio to IO formation in reaction (R8), which was taken as 0.86 from a study of the same group [26]. Similar to the present experiments, analysis of the IO profile using numerical simulation also took into account the formation kinetics of IO to yield a cross-section of $(3.6 \pm 0.5) \times 10^{-17}$ cm^2 molecule^{-1} at a resolution of 0.14 nm.

Experiments were also performed in which O_3 was dissociated at 248 nm (R12) to form $O(^3P)$, which then reacted with I_2 (R7). In this case IO was monitored at high resolution using the diode laser (at the maximum of the 4,0 band) and calibration of the laser fluence was carried out by photolysing HNO_3 at the same wavelength and monitoring NO_2 formation (using the same diode laser), resulting in a cross-section of $(3.4 \pm 0.4) \times 10^{-17}$ cm^2 molecule^{-1}. These experiments were carried out using low concentrations of O_3 and $O(^3P)$ to avoid problems with aerosol generation upon mixing O_3 and I_2. In contrast to the work of Sander [43], Harwood et al. [28] did not find a measurable dependence of the cross-section on temperature.

Bloss et al. [12] made measurements of the IO cross-section using a monochromator/CCD set-up that enabled measurement of transient absorption at multiple wavelengths to be made simultaneously. IO was generated using N_2O photolysis and reaction of $O(^3P)$ with CF_3I ((R16) followed by (R8)). These authors adopted a branching ratio of $k_{8a}/k_8 = 0.845$ from the work of Gilles et al. [26]. Bloss et al. [12] measured the relative yield of IO under various conditions and found it to be pressure dependent at low temperatures, but not at 295 K, implying a temperature dependence in the value of the branching ratio k_{8a}/k_8. The cross-sections of IO determined by these authors therefore showed a temperature dependence, which was much weaker than that observed by Sander [43] but still inconsistent with the temperature independent cross-sections of Harwood et al. [28].

The data summarised in Table 4 reveals significant differences in the cross-section determinations in the various studies reported, with values between 1.9 and 3.6×10^{-17} cm^2 molecule^{-1} reported. The origin of this apparent poor agreement may be spectroscopic or chemical in nature. An examination of Fig. 2 shows that the 4,0 band is rather asymmetric, with a very steep short-wavelength flank. A wavelength error can thus have a significant impact on the cross-sections obtained, especially if the offset is to smaller wavelengths. As discussed above this is a potential explanation for the low value obtained by Jenkin and Cox [42]. The cross-section of Bloss et al. [12] is even lower, and this can be only partially attributed to the effect of spectral resolution. As shown in Fig. 4, when using a central wavelength of 427.2 nm, the effect of reducing resolution from 0.1–0.2 to 1.13 nm would be to decrease the cross-section at 427.2 nm by >30% although we recognise that the correction factor would vary between optical set-ups due to different entrance slit functions and the use of either diode array or photomultiplier located behind an exit slit as detector.

A correction of this size would however still leave the cross-sections of Bloss et al. [12] rather low, leaving us to conclude that chemical effects may also have played a role. In this context, we note that the experiments of Bloss et al. [12] generally

used significantly higher initial concentrations of IO than e.g. Harwood et al. [28], Laszlo et al. [30] or the present study, which will lead to a more rapid decay of IO and probably to a complex chemical situation. The origin of the apparently low cross-section of Laszlo et al. [30] may be found by examining the calibration scheme, which used the change in optical density due to I_2. The authors used a cross-section of I_2 at 530 nm of 2.56×10^{-18} cm^2 molecule^{-1}, which is considerable smaller than the cross-sections of Tellinghuisen [32] at this wavelength (3.09×10^{-18} cm^2 molecule^{-1}), which form the basis of the IUPAC recommendation [34] for this spectrum. Use of the correct I_2 cross-sections results in a value of $(3.4 \pm 0.5) \times 10^{-17}$ cm^2 molecule^{-1} from the study of Laszlo et al. [30]. If we also take into account that the Laszlo et al. [30] data were obtained at lower resolution, we can correct their cross-section using the data in Fig. 4 upwards by ≈5% to derive a final number of $\sigma = (3.6 \pm 0.6) \times 10^{-17}$ cm^2 molecule^{-1} at 427.2 nm.

The somewhat low value of Stickel et al. [17] may also be related to the calibration scheme which employed physical rather than chemical measurement of the laser fluence (i.e. calibrated power meter instead of in situ chemical actinometry).

It is difficult to find potential sources of systematic error in the work of Sander [43], which, on paper, uses a very simple chemical scheme to generate and calibrate the IO signal. The use of a short wavelength flash lamp to dissociate O_2 would certainly have generated large I atom concentrations in their set-up, though it is unclear how this may have influenced the cross-section determination. Only the strong temperature dependence of the IO cross-sections may be indicative of systematic error.

4.3. Recommendations

In order to make a recommendation for the IO cross-section at 298 K and at the peak of the 4,0 band we consider the data of Harwood et al. [28], Laszlo et al. [30] and the present study, all obtained by laser photolysis, to be the most reliable. The cross-section at the peak of the 4,0 band from these studies is $(3.6 \pm 0.5) \times 10^{-17}$ cm^2 molecule^{-1} (Harwood et al. [28]), $(3.8 \pm 0.7) \times 10^{-17}$ cm^2 molecule^{-1} (Laszlo et al. [30], recalculated using the Tellinghuisen [32] cross-section for I_2 at 530 nm, and scaled as described in Table 4) and $(3.8 \pm 0.4) \times 10^{-17}$ cm^2 molecule^{-1} from the present study (scaled by a factor of 1.08 to take into account the ratio of cross-sections at λ_{max} and 427.2 nm). Considering that several different chemical schemes were used to generate the radical, these data are in reasonable agreement. An average value of $\sigma^{IO}(4,0) = (3.7 \pm 0.4) \times 10^{-17}$ cm^2 molecule^{-1} from these studies would appear to represent the best available cross-section to date and is still consistent within the error bars with the data obtained by both Stickel et al. [17] and Sander [43].

5. Conclusions

Three different chemical schemes were used to generate to IO in order to determine the shape of the 4,0 band and the absorption cross-section at 427.2. The cross-section obtained in this work, $\sigma^{IO}_{427.2\,nm} = (3.55 \pm 0.35) \times 10^{-17}$ cm^2 molecule^{-1} confirms the results of selected recent studies, and strengthens the spectroscopic database on this radical. Disagreements in the literature values for IO cross-sections have largely been resolved and the most reliable studies identified, thus enabling a recommendation to be made.

Acknowledgements

We would like to thank J. Burkholder for provision of the raw data of the 4,0 band of Harwood et al. [28] and for personally communicating details of their experimental procedure. We thank T. Gravestock for useful discussions related to LIF detection of vibrationally excited IO and R.A. Cox, M.E. Jenkin and S.P. Sander for personally communicating details of their experimental procedure. We thank DJC for some help with the data analysis. This work was conducted within the framework of the EU project "THALOZ" (EVK2-CT-2001-00104) and the BMBF AFO-2000 project "REHATROP". M.E.T was supported by the Fundación Antorchas, Consejo Nacional de Investigaciones Científicas y Técnicas (CONICET) and the "Deutscher Akademischer Austausch Dienst" (DAAD).

References

[1] B.J. Allan, G. McFiggans, J.M.C. Plane, H. Coe, J. Geophys. Res. 105 (2000) 14363–14369.
[2] B. Alicke, K. Hebestreit, J. Stutz, U. Platt, Nature 397 (1999) 572–573.
[3] U. Frieß, T. Wagner, I. Pundt, K. Pfeilsticker, U. Platt, Geophys. Res. Lett. 28 (2001) 1941–1944.
[4] L.J. Carpenter, W.T. Sturges, S.A. Penkett, P.S. Liss, B. Alicke, K. Hebestreit, U. Platt, J. Geophys. Res. 104 (1999) 1679–1689.
[5] A. Saiz-Lopez, J.M.C. Plane, Geophys. Res. Lett. 31, doi:10.1019/2003GL019215, 2004.
[6] C.M. Roehl, J.B. Burkholder, G.K. Moortgat, A.R. Ravishankara, P.J. Crutzen, J. Geophys. Res. 102 (1997) 12819–12829.
[7] A. Saiz-Lopez, R.W. Saunders, D.M. Joseph, S.H. Ashworth, J.M.C. Plane, Atmos. Chem. Phys. 4 (2004) 1443–1450.
[8] S.A. Carl, J.N. Crowley, Atmos. Chem. Phys. 1 (2001) 1.
[9] E.S.N. Cotter, N.J. Booth, C.E. Canosa-Mas, D.J. Gray, D.E. Shallcross, R.P. Wayne, Phys. Chem. Chem. Phys. 3 (2001) 402–408.
[10] D. Bauer, T. Ingham, S.A. Carl, G.K. Moortgat, J.N. Crowley, J. Phys. Chem. 102 (1998) 2857–2864.
[11] D. Davis, J. Crawford, S. Liu, S. McKeen, A. Bandy, D. Thornton, F. Rowland, D. Blake, J. Geophys. Res. 101 (1996) 2135–2147.
[12] W.J. Bloss, D.M. Rowley, R.A. Cox, R.L. Jones, J. Phys. Chem. A 105 (2001) 7840–7854.
[13] N.S. Holmes, J.W. Adams, J.N. Crowley, Phys. Chem. Chem. Phys. 3 (2001) 1679–1687.
[14] J.C. Mössinger, R.A. Cox, J. Phys. Chem. A 105 (2001) 5165–5177.
[15] G. Inoue, M. Suzuki, N. Washida, J. Chem. Phys. 79 (1983) 4730–4735.
[16] E.H. Coleman, A.G. Gaydon, W.M. Vaida, Nature 162 (1948) 108–109.
[17] R.E. Stickel, A.J. Hynes, J.D. Bradshaw, W.L. Chameides, D.D. Davis, J. Phys. Chem. 92 (1988) 1862–1864.
[18] A.A. Turnipseed, M.K. Giles, J.B. Burkholder, A.R. Ravishankara, Chem. Phys. Lett. 242 (1995) 427–434.
[19] D.B. Atkinson, J.W. Hudgens, A.J. Orr-Ewing, J. Phys. Chem. 103 (1999) 6173–6180.
[20] Y. Nakano, S. Enami, S. Nakamichi, S. Aloisio, S. Hashimoto, M. Kawasaki, J. Phys. Chem. A 107 (2003) 6381–6387.
[21] T. Ingham, M. Cameron, J.N. Crowley, J. Phys. Chem. 104 (2000) 8001–8010.

[22] M. Wollenhaupt, S.A. Carl, A. Horowitz, J.N. Crowley, J. Phys. Chem. A 104 (2000) 2695–2705.
[23] T.J. Dillon, R. Karunanandan, J.N. Crowley, in preparation.
[24] M.E. Tucceri, T.J. Dillon, J.N. Crowley, Phys. Chem. Chem. Phys. 7 (2005) 1657–1663.
[25] M.A. Teruel, T.J. Dillon, A. Horowitz, J.N. Crowley, Phys. Chem. Chem. Phys. 6 (2004) 2172–2178.
[26] M.K. Gilles, A.A. Turnipseed, R.K. Talukdar, Y. Rudich, P.W. Villalta, L.G. Huey, J.B. Burkholder, A.R. Ravishankara, J. Phys. Chem. 100 (1996) 14005–14015.
[27] L.T. Molina, M.J. Molina, J. Geophys. Res. 91 (1986) 14501–14508.
[28] M.H. Harwood, J.B. Burkholder, M. Hunter, R.W. Fox, A.R. Ravishankara, J. Phys. Chem. A 101 (1997) 853–863.
[29] B. Edlén, Metrologia 2 (1966) 71–80.
[30] B. Laszlo, M.J. Kurylo, R.E. Huie, J. Phys. Chem. 99 (1995) 11701–11707.
[31] J.P. Burrows, A. Dehn, B. Deters, S. Himmelmann, A. Richter, S. Voigt, J. Orphal, J. Quant. Spec. Radiat. Transf. 60 (1998) 1025–1031.
[32] J. Tellinghuisen, J. Chem. Phys. 58 (1973) 2821–2834.
[33] S.P. Sander, R.R. Friedl, D.M. Golden, M.J. Kurylo, R.E. Huie, V.L. Orkin, G.K. Moortgat, A.R. Ravishankara, C.E. Kolb, M.J. Molina, B.J. Finlayson-Pitts, Chemical kinetics and photochemical data for use in atmospheric studies, evaluation number 14, in: Jet Propulsion Laboratory, 2003.
[34] R. Atkinson, D.L. Baulch, R.A. Cox, J.N. Crowley, R.F. Hampson, R.G. Hynes, M.E. Jenkin, J.A. Kerr, M.J. Rossi, J. Troe, IUPAC Subcommittee for gas kinetic data evaluation. Evaluated kinetic data: http://www.iupac-kinetic.ch.cam.ac.uk/, 2005.
[35] A. Misra, P. Marshall, J. Phys. Chem. 102 (1998) 9056–9060.
[36] T.J. Dillon, D.E. Heard, J. Photochem. Photobiol. 157 (2003) 223–230.
[37] E.P. Daykin, P.H. Wine, J. Phys. Chem. 94 (1990) 4528–4535.
[38] R.A. Durie, F. Legay, D.A. Ramsay, Can. J. Phys. 38 (1960) 444.
[39] R.A. Durie, F. Legay, D.A. Ramsay, Spectrochim. Acta 15 (1959) 749.
[40] R.A. Durie, D.A. Ramsay, Can. J. Phys. 36 (1958) 35.
[41] R.A. Cox, G.B. Coker, J. Phys. Chem. 87 (1983) 4478–4484.
[42] M.E. Jenkin, R.A. Cox, J. Phys. Chem. 89 (1985) 192–199.
[43] S.P. Sander, J. Phys. Chem. 90 (1986) 2194–2199.
[44] B.J. Allan, J.M.C. Plane, J. Phys. Chem. A 106 (2002) 8634–8641.